RESEARCH Revista Mexicana de Física **64** (2018) 61–66 JANUARY-FEBRUARY 2018

Optical characterization of CdTe nanoparticles embedded in a nanoparticulate SnO_2 matrix

E. Campos-González[a,b], M. Becerril[b], J. Santoyo-Salazar[b], H. Silva-López[b], F. de Moure Flores[a],
and O. Zelaya-Ángel[b,*]
[a]*Facultad de Química, Materiales, Universidad Autónoma de Querétaro,*
Querétaro, 76010, México.
[b]*Departamento de Física, Centro de Investigación y de Estudios Avanzados del I.P.N.*
Apartado Postal 14-740, México D.F. 07360, México.
e-mail: ozelaya@fis.cinvestav.mx

Received 14 August 2017; accepted 2 October 2017

Cadmium telluride (CdTe) nanoparticles were grown in the interior of a SnO_2 transparent matrix by means of the r.f. sputtering technique. X-ray diffraction (XRD) patterns reveal that the CdTe quantum dots (QD) grow in the hexagonal wurtzite (W) phase. Diffraction data show that SnO_2 is constituted by nanoparticles also, with size of the same order of the W-CdTe QD. The broad bands of the XRD patterns and the Scherrer formula allowed, by assuming a spherical shape, the W-CdTe QD size calculation, which have average diameters in the range 4.8 - 14.0 nm. These data were confirmed by electron microscopy images. Optical absorbance gives information to calculate the energy of the two lowest excitonic states (band gap). The Raman spectra show several broad bands in the range 100 - 200 cm^{-1}, on which deconvolution allows separate five modes in the 100 - 200 cm^{-1} interval. The bands correspond to CdTe and tetragonal Te. The transversal optic (TO) and longitudinal optic (LO) modes of CdTe at the Γ point of the first Brillouin zone, for phonons in nanoparticles, follow the expected behavior if the radius of crystal decreases, taking into account that the selection rules for momentum conservation are relaxed.

Keywords: Semiconductors; quantum dots; Raman; II-VI.

PACS: 81.07.-b; 81.07.Ta; 78.30.-j; 81.05.Dz

1. Introduction

CdTe semiconductor nanoparticles immersed in transparent matrices have currently many important applications in electrochemistry [1], photoelectricity [2], solar cells fabrication [3], chemical sensors [4], bio-labelling [5] etc. The achievement of desired particle sizes over the largest possible range, controlled particular sizes, and good crystallinity are some of the properties expected in nanocrystal growing methods. The transparent matrices can be solid or liquid and organic or inorganic, depending on their use and the growth method employed. Thus, hard matrices for CdTe such as silica [6] and soft ones like hydrogels [7] have been employed, which allow a large variety of applications. SnO_2 is a transparent oxide with the property of possessing high electric conductivity that places the oxide in a special position as matrix for electronic devices design, as instance. At present, CdS nanoparticles embedded in SnO_2 have been successfully utilized in photocurrent generation [8], and in solar cells based on CdTe nanoparticles immersed in SnO_2 matrix have been already studied with good results [9]. Nowadays, a lot of growing techniques exist, physical or chemical, to prepare semiconducting nanoparticles, which have found a great acceptance among the researches of wide-world. In the last four years several works have been publishe about CdTe nanoparticles immersed in SiO_2, in which the good photoluminescent properties at energies larger than that of bulk CdTe have been reported [10–12].

In this work the preparation of CdTe nanoparticles by means of r.f. sputtering with radius in the range 2.4 - 7.0 nm is reported. Actually, a CdTe-SnO_2 nanocomposite was grown on glass substrates. Within the framework of II-VI semiconductor quantum dots (QD) the sputtering growth technique offers controlled size distribution, also the preparation of CdTe crystallized in the metastable hexagonal wurtzite phase [13]. Structural and optical studies include X-ray diffraction, transmission electron spectroscopy, optical absorption and Raman analysis to characterize the quantum confinement in the CdTe nanoparticles immersed in the also nanoparticulate SnO_2 matrix, both undoped. The variation at room temperature (RT) of the main vibrational modes of wurtzite CdTe nanoparticles, when their size goes to small values, is studied. The main contribution of this the analysis of the optical properties of hexagonal CdTe, since there are few reports in this crystalline phase of this important semiconductor.

2. Experimental Details

The CdTe + SnO_2 thin films were prepared on 7059 Corning glass substrates by means of the r.f. sputtering technique in an Ar ambient at 20 mTorr and at RT. The time for deposition was 180 min. The target was 5 cm^2 of diameter and was prepared with mixed 99.999 % purity SnO_2 and CdTe powders. The CdTe weight percentage in the target varied from 2% to 20% to get different nanoparticles size. After the growth the

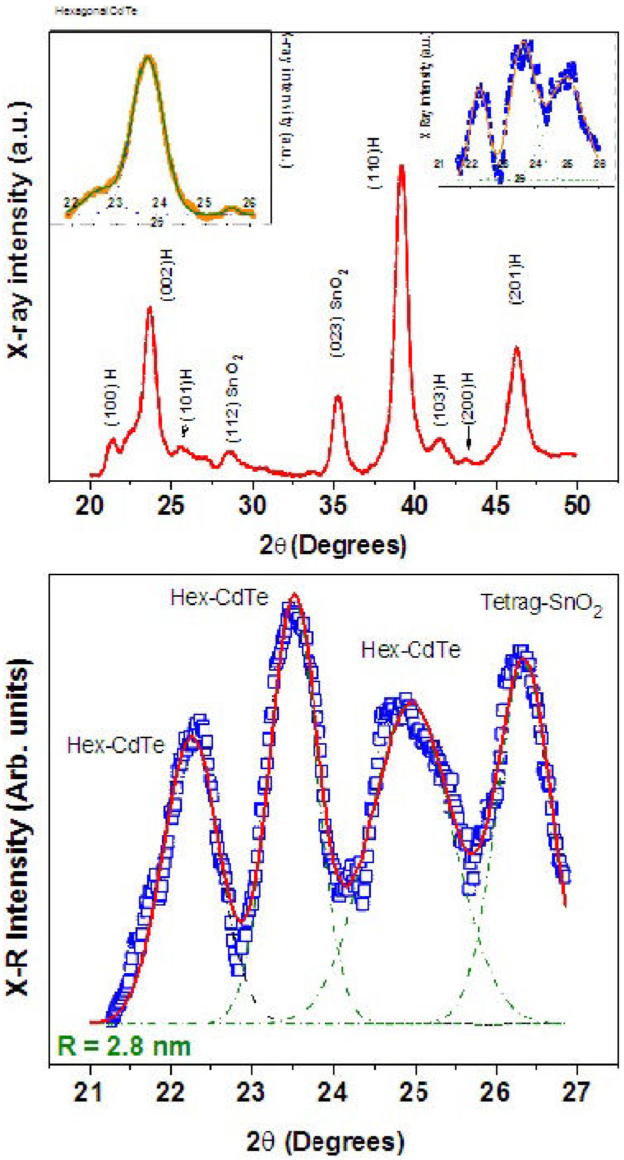

FIGURE 1. (a) Typical X ray diffraction (XRD) pattern of the W-CdTe embedded in SnO_2 matrix. Reflections labeled with H indicates CdTe in hexagonal wurtzite crystalline phase. XRD peaks corresponding to the tetragonal phase of the SnO_2 matrix can be observed. Insets illustrate the deconvolution fitting process followed to calculate the nanoparticle radius. (b) Deconvolution of hexagonal CdTe and SnO_2 broad X-ray diffraction bands. In this picture it can be appreciated that both types of nanoparticles have approximated the same average size.

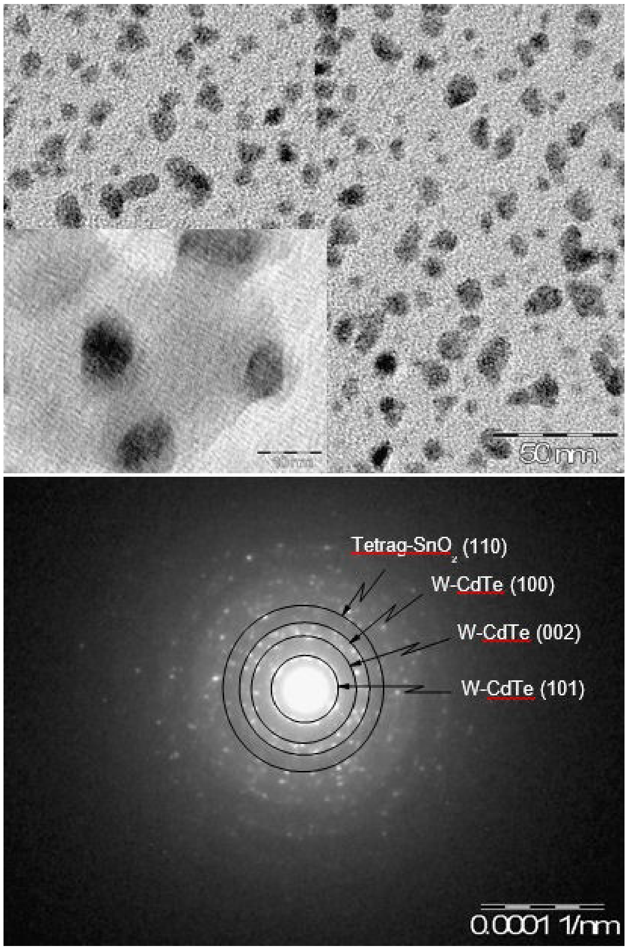

FIGURE 2. (a)TEM image of CdTe distribution of nanoparticles immersed in the SnO_2 matrix for an average diameter of $\sim$ 12 nm. The inset illustrates the TEM image of a detail of CdTe QD prepared with average size of $\sim$ 4 nm, the bar scale is 10 nm. (b) Electron diffraction pattern of nanoparticulate W-CdTe and SnO_2 matrix.

samples were annealed at 300°C in air during one hour. A variety of different crystallite size in the 4.8 - 14 nm range was obtained. Films have thickness of 200 ± 20 nm, as measured by using a Dektak II profilometer. For the crystalline structure analysis an X-ray Diffractometer Siemens D5000 (Cu-Kα radiation) was utilized. The size of nanoparticles was determined by employing the Scherrer formula and transmission electron microscopy (TEM) images. TEM apparatus employed was a Jeol 2010 working at 200 KeV. The CdTe + SnO_2 layers were detached from the substrate and attached onto the TEM-grills. Indexation was computed by the relation $d_t = \lambda_t L_t/r_t$ where $\lambda_t = 0.0027$ nm is the electron wavelength at 200 keV, the steady camera for diffraction with L_t = 30 cm, and where r_t (mm) is the radius measured from the transmitted electron beam to the diffracted rings (Fig. 2b). Data were taken, from selected area of electron diffraction (SAED) and x-ray diffraction (XRD) patterns, to define the structure by Diamond 3.0 software. The band gap and higher electronic transitions were measured from optical absorption spectra (OA). OA spectra were measured by means of a UNICAM 8700 spectrophotometer. The Raman spectra of the samples were measured at room temperature with the LabRaman II Dilor spectrometer with excitation light of 514 nm wavelength. All the characterization was performed at RT.

3. Results and Discussion

The crystalline structure of the CdTe nanoparticles immersed in SnO_2 is the hexagonal wurtzite (W-CdTe) phase as ob-

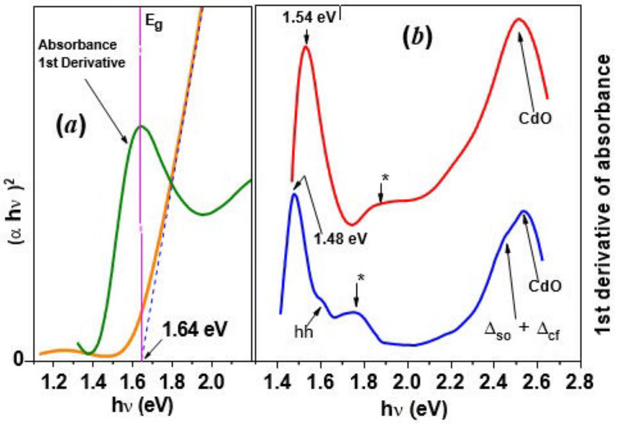

FIGURE 3. (a)Calculation of the first exited energy of electrons in the nanoparticle with $R = 4.5$ nm employing both the first derivative of absorbance spectra and the $(\alpha h\nu)^2 = A(E_{g-\mathrm{nano}} - h\nu)$ formula. (b) First derivative of absorbance of two samples, the first maximum indicates the position of the first quantized energy level. Arrows with asterisks as superindex indicate the energy of the second quantized energy level.

served in Fig. 1(a), where a typical XRD pattern of the CdTe + SnO$_2$ nanocomposite, in the range $20 \leq\ 2\theta \leq\ 50$ degrees, is exhibited. XRD peaks which correspond to the tetragonal crystalline phase of SnO$_2$, the matrix, are also observed in Fig. 1(a). In the two insets of this figure are displayed in detail, in the interval $2\theta = 22 - 25$ degrees, W-CdTe diffractograms with three reflections. These nearby three XRD signals can be considered as the finger print of the wurtzite phase of many materials which crystallize in hexagonal packing. Wurtzite is a metastable phase for CdTe, however, Farias *et al*. have demonstrated that, from the thermodynamic point of view, wurtzite phase should be more stable than the zinc blende for very small radius nanoparticles [14]. The samples studied here were deposited at $\sim\ 1.1$ nm/min, which can be considered as a very slow growing rate, in such a way that it enables the nanoparticles to grow, practically, in equilibrium conditions at RT. The XRD reflections of the SnO$_2$ do not always appear in the low 2θ values region, probably there the reflections are so weak because the existence of preferred orientation in other crystallographic directions. In Fig. 1(b), an XRD reflection of SnO$_2$ can be observed together with the triplet of W-CdTe. This diffractogram indicates that the size of SnO$_2$ nanoparticles is of the same order of the size of the CdTe ones. In order to calculate the average radius R of the nanoparticles, a deconvolution process with Gaussian profiles was carried out to determine the full width at half maximun (FWHM) of the XRD bands. This step allows obtain the center of each band also. The average radius of the particles, obtained from the Scherrer's formula and from FWHM values of the bands in XRD patterns of a set of ten CdTe nanoparticles, lies in the 2.4 - 7.0 nm range. The TEM image of the CdTe-QD distribution grown with $R = 6.0 \pm 0.7$ nm into the SnO$_2$ matrix is displayed in Fig. 2(a), the inset illustrates the TEM image nanoparticles with $R = 4.0\pm$ 0.5 nm. In Fig. 2(b) the electron diffraction pattern of the CdTe nanoparticles plus the SnO$_2$ nanoparticulate matrix is exhibited, where the pattern clearly evidences that CdTe nanoparticles have grown with the hexagonal symmetry.

From the UV-Vis optical absorption spectra of the CdTe + SnO$_2$ films and the relation $(\alpha h\nu)^2 = A(E_{g-\mathrm{nano}} - h\nu)$ the first electronic transition, *i.e.*, the direct energy band gap ($E_{g-\mathrm{nano}}$) was obtained for the samples. Here, α is the optical absorption coefficient, h the Plank's constant, ν the photon frequency, $h\nu$ the photon energy, and A a constant. In Fig. 3(a) is shown the calculation of $E_{g-\mathrm{nano}}$ for the sample prepared with $R = 4.6 \pm 0.4$ nm, where the extrapolation of the linear part of the curve until the $h\nu$ axis indicates that $E_{g-\mathrm{nano}} = 1.64$ eV. In this same panel the first derivative with respect to $h\nu$ of the absorbance [d(OA)/d($h\nu$)] as a function of $h\nu$ is outlined (thin line). The position of the maximum of d(OA)/d($h\nu$) on the $h\nu$ axis coincides with the value of E$_g$ formerly calculated. Thus, the first derivative of OA will be used to estimate with good approximation all the electronic transition data, as has been used for other authors [15]. Furthermore, the d(OA)/d($h\nu$) lineshape allows observe other transitions with better resolution. In Fig. 3(b) d(OA)/d($h\nu$) of two samples is displayed, the position of the first electronic transition is indicated with the first maximum.

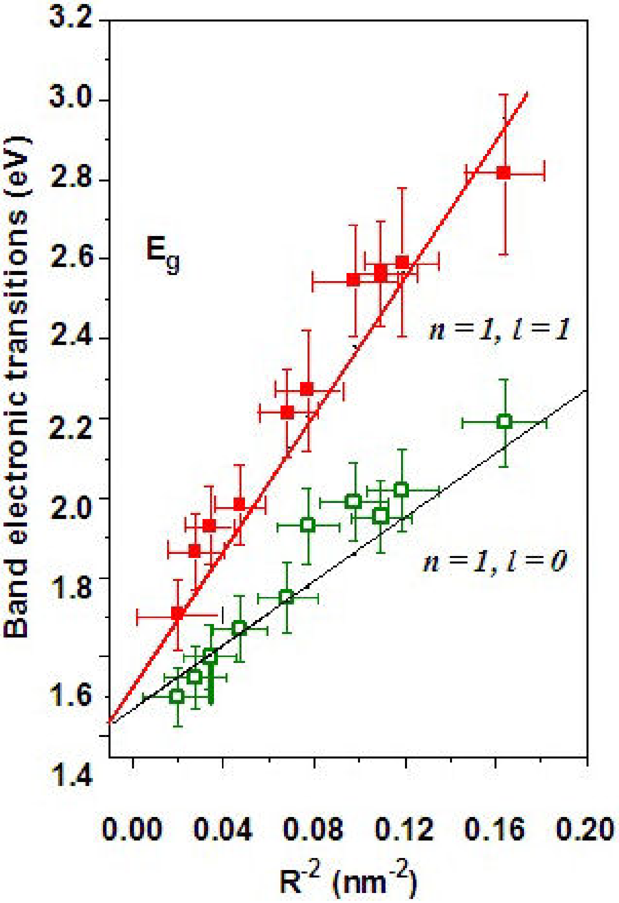

FIGURE 4. First two electronic transitions of W-CdTe versus the square inverse of nanoparticle radius.

The second electronic transition due to the next discrete level has been identified with the second band and was indicated with other small arrow accompanied by an asterisk. The third transition observed in Fig. 3(b) is a well pronounced maximum around 2.5 eV, which has been identified by us that is originated from CdO formed at the interface CdTe-SnO_2 [16], since the direct band gap of CdO is ~ 2.5 eV [17]. Other possible phases formed in the CdTe surface [14] as product of oxidation are TeO_2 and $CdTeO_3$ [16, 18], however these oxides have band gap values of $\sim$ 3.8 and ~ 3.9 eV, respectively [19-22]. Then, in our case, that a CdO layer has been formed in the CdTe/SnO_2 interface is highly probable. A small feature in the bottom spectrum in Fig. 3(b), which was indicated by the "*hh*" label, is due to first electronic transition from the heavy-holes in the valence band [23]. In this same spectrum a shoulder is observed at around 2.44 eV which is due to the spin- orbit plus the crystal field unfolding $(\Delta_{so} + \Delta_{cf})$. The values $\Delta_{so} = 93$ meV and $\Delta_{cf} = 3$ meV have been reported for W-CdTe [24, 25]. The last unfolding arises because here CdTe has hexagonal symmetry [26]. For high energy values ($E_{g-\text{nano}} \geq 1.64$ eV) a deconvolution process was applied to have a better definition of the position of the second electronic transition.

The first ($E_{g-\text{nano}}$) and the second electronic transitions as a function of the inverse square radius of QD are displayed in Fig. 4. Despite the scattering of the experimental points, it can be concluded that both electronic transitions satisfy the well known E_g versus R^{-2} dependence. The solid lines on the experimental data have been drawn according with the relation $E_{n,l}$(R) = E$_g$+$(\nabla^2/2R^2)$[$(x_{n\ e,le})^2/m_e$ + $(x_{nhlh})^2/m_h$], where *n*, *l* are the electron or hole eigenstates as 1s, 1p, 1d, etc. $E_g = 1.43$ eV is the band gap energy of the bulk CdTe at RT, m_e and m_h are the effective masses of electron and holes, respectively. x_{n_e,l_e}, x_{n_h,l_h} are the roots of the spherical Bessel functions [27,28]. The Bohr Radius of CdTe is 7.3 nm, which means that our analysis has been totally developed in the strong quantum confinement regime. The optical properties of absorbance and photoluminescence of the CdTe nanoparticles do not overlap with those of SnO_2 because the difference in the band gap values ($E_g = 3.8$ eV for bulk SnO_2).

High resolution of CdTe Raman spectra was carried out in the set of samples. The Raman spectra of two CdTe representative samples (samples with $R = 5.4 \pm 0.4$ and 2.4 ± 0.5 nm) in the range 100-400 cm^{-1} are depicted in Figs. 5(a) and 5(b), respectively. In both cases the deconvolution process with Lorentzian curves of the spectrum is also illustrated. Five modes are observed in the Raman spectra of CdTe in the 100 - 170 cm^{-1} range. The modes which practically coincide are those of E_2-Te and TO-CdTe, both at $\sim$ 140 cm^{-1}. However, in past we have found that the TO-CdTe mode lies slightly at low energies of E_2-Te [29]. A lower vibrational band observed at slightly low energy than $\sim$ 140 cm in CdTe nanocrystals, has been associated to DALA mode (disorder activated longitudinal acoustic) by other authors [30]. In Figs. 5(a) and 5(b) the mode E_2-Te has been fitted at lower energy than that of TO-CdTe. The mode at The Raman spectrum of CdTe has been The modes centered at ~ 140 and ~ 160 cm^{-1} correspond to the transversal optic (TO) and to the longitudinal optic (LO) vibrational modes of cubic and hexagonal CdTe, respectively [31–33], and the mode located at about 120 cm^{-1} has been associated to with the A_1(TO) of hexagonal Te [33, 34]. The positions of the centers of both the TO and the LO modes of CdTe as a function of *R* are shown in Fig. 6(a). The most important modes in nanometric SnO_2 are observed at wavenumbers above the 450 cm^{-1} [35]. Even with the large scattering of experimental points, a tendency of the LO mode to soften and the TO mode to harden can be ensured. In Fig. 6(b) the dispersion curves of cubic zincblende CdTe in the 160-180 cm^{-1} interval are shown [34, 35]. No specific information exists in the literature about the dispersion curves of the hexagonal wurtzite CdTe, nevertheless, given the similarities

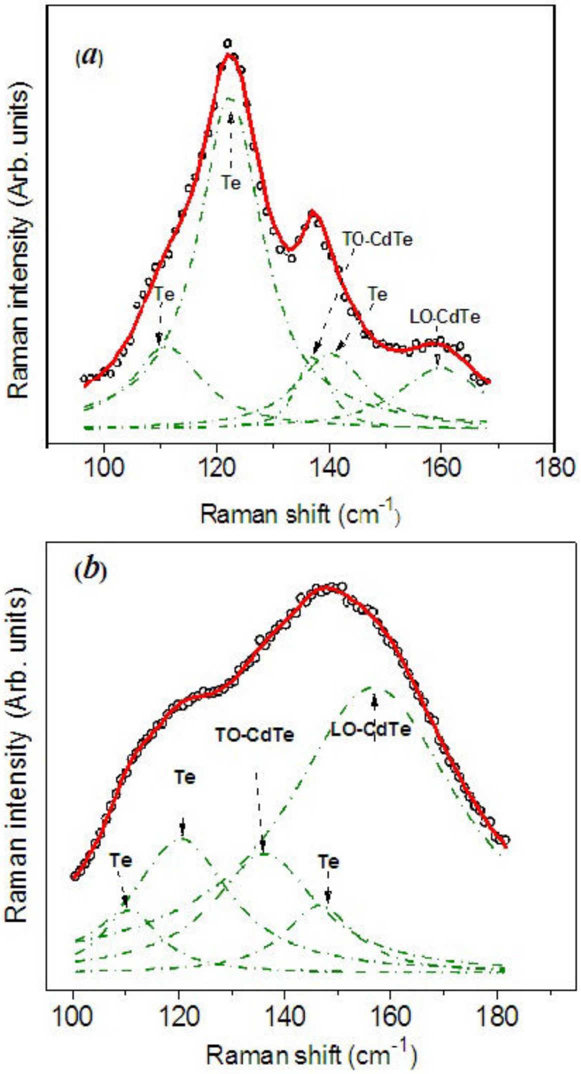

FIGURE 5. Raman spectra of two CdTe nanoparticles. (a) Deconvolution to separate the positions of the modes of Te and of the TO and LO modes of the CdTe nanoparticle with $R = 5.4$ 0.4 nm. (b) Of sample with $R = 2.4$ 0.5 nm.

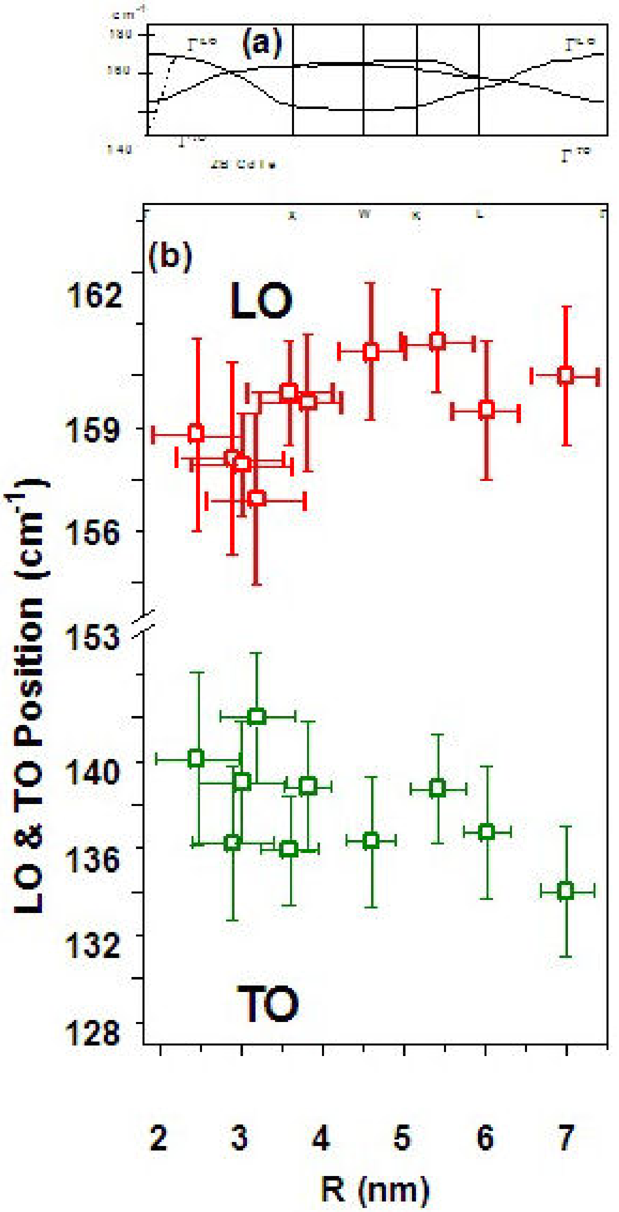

FIGURE 6. (a) Section of the dispersion curves of cubic-zincblende CdTe found in the literature. (b) Positions of the LO and TO modes of the W-CdTe nanoparticles as a function of the particle radius.

existent between hexagonal-Wurtzite (HW) and cubic-Zinc blende (CZB) crystalline phases, the unit cell length of HW along the (0001) axis is double with respect to CZB along the (111) direction (Γ → L) [36]. The dispersion curves of CZB along the Γ-X and Γ-L, high symmetry directions, of the 1st Brillouin zone can be used to analyze the variation of the TO and LO modes around the Γ point when R decreases. The very low dimensional character of nanoparticles breaks the translational periodicity, then, the selection rules of crystal momentum conservation are relaxed when $R\rightarrow 0$, the momentum conservation is less and less preserved. Then, transitions out the Γ point are allowed, as outlined by the dashed arrow in Fig. 6(b). In this way, as R goes to lower values, the dashed arrow can move away the Γ point more and more. This fact indicates that when R decreases LO decreases, and on the contrary, TO increases. The shift to lower frequency values of the LO mode of CdTe when R decreases has been observed by Rolo *et al* [27]. This behavior is consequence of quantum confinement effects. Theoretically, Trallero-Giner *et al*. have developed a model for the LO mode of CdS for nanocrystals, in which the mode is softens when nanoparticles size decreases [37].

4. Conclusions

Wurtzite CdTe nanoparticles embedded in SnO$_2$ matrix in the radius range 2.4-7.0 nm were succesfully prepared by means of the r.f. sputtering technique. X-ray diffraction shows that W-CdTe and Tetragonal SnO$_2$ nanocrystals have sizes of the same order. W-CdTe is the metastable phase of bulk CdTe, however for nanoparticles is a stable phase. The quantum confinement occurs in the strong regime as the Bohr radius for CdTe is 7.3 nm. From optical absorbance the first and second electronic transition were determined. In Raman spectra the LO and TO modes of W-CdTe were measured where, as expected from dispersion curves, the LO mode hardens and the TO softens when the radius of nanoparticles tends to lower values.

Acknowledgements

The authors thank to M. Guerrero and A. García for their technical assistance. The authors acknowledge financial support for this work from FONDO SECTORIAL CONACYT-SENER-SUSTENTABILIDAD ENERGÉTICA through CeMIE-sol, within of the strategic project number 37; "Development of new photovoltaic devices and semi-superconductor materials". E. Campos-Gonzáles also acknowledges CONACyT-México for support underprogram "Estancias Posdoctorales Nacionales".

---

1. Y. Bae, N. Myung, and A.J. Bard, *Nano Letters* **4** (2004) 1153.
2. J.A. Seabold *et al*., *Chemistry of Materials* **20** (2008) 5266.
3. D. Verma, A. Ranga Rao, and V. Dutta, *Solar Energy Materials ana Solar Cells* **93** (2009) 1482.
4. M.F. Frasco and N. Chanotakis, *Sensors* **9** (2009) 7266.
5. M. Green *et al*., *Journal of Materials Chemihtry* **17** (2007) 1989.
6. E. Mota-Pineda and M. Melendez-Lira, *Journal of Applied Physics* **104** (2008) 064316.

7. E. Kharlampieva *et al*., *Soft Matter* **6** (2010) 800.
8. C. Nasr, S. Hotchandani, W.Y. Kim, R.H. Schheml, and P.V. Kamat, *Journal of Physical Chemistry B* **101** (1997) 7480.
9. M. Pehnt *et al*., *AIP Conferences Proceedings* **353** (1996) 384.
10. S. Zhang *et al*., *Part. Syst. Charact.* **33** (2016) 261-270.
11. L. Tang *et al*., *Optic Express* **21** (2013) 11095-11100.
12. O.G. Morales-Saavedra, C.D. Gutiérrez-Lazos, M. Ortega-López, and A.A. Rodriguez-Rosales, *J. Appl. Res. Technol.* **13** (2015) 566-575.
13. P.M.A. de Farias, B.S. Santos, R.I. Longo, R. Ferreira, and C.L. Cesar, *Materials Chemistry and Physics* **89** (2005) 21.
14. M. Becerril *et al*., *Journal of Crystal Growth* **311** (2009) 1245.
15. A.C. Rastogi, S.N. Sharma, and S. Kohli, *Semiconductors Science and Technology* **15** (2000) 1011.
16. Y. Zhang *et al*., *Journal of the American Chemical Society* **128** (2006) 13396.
17. J. Santos-Cruz *et al*., *Thin Solid Films* **493** (2005) 83.
18. P. Babu Dayal, B.R. Mehta, Y. Aparna, and S.M. Shivaprasad, *Applied Physics Letters* **81** (2002) 4254.
19. F.J. Espinoza-Beltran *et al*., *Journal of Vaccum Science and Technology A* **11** (1993) 3062.
20. E. Menéndez-Proupin, G. Gutiérrez, E. Palmero, and J.L. Peña, *Physical Review B* **70** (2004) 035112.
21. M.Y. El Azharia *et al*., *Thin Solid Films* **366** (2000) 82.
22. T. Siciliano *et al*., *Sensor and Actuators B: Chemistry* **137** (2009) 644.
23. V. Esch *et al*., *Physical Review B* **42** (1990) 7450.
24. P. Lefebvre, T. Richard, J. Allegre, and H. Mathieu, *Phyrical Review B* **53** (1996) 15440.
25. P. Babu Dayal, B.R. Mehta, and P.D. Paulson, *Physical Review B* **72** (2005) 115413.
26. O. Portillo-Moreno, O. Zelaya-Angel, R. Lozada-Morales, M. Rubin-Falyan, and J.A. Rivera-Marquez, *Optical Materials* **18** (2002) 383.
27. L.E. Brus, *Journal of Chemical Physics* **79** (1983) 5566.
28. M.H. Yükselici and Ç. Allahverdi, *Physica Status Solidi B* **236** (2003) 694.
29. J.G. Quiñones-Galván *et al*., *J. Appl. Phys.* **118** (2015) 125304-6.
30. N. Devki Talwar, Zhe Chuan Feng, Jyh-Fu Lee, and P. Becla, *Mater. Res. Express* **1** (2014) 015018-11.
31. J. Huerta, M. Lopez, and O. Zelaya-Angel, *Journal of Vacuum Science and Technology B* **18** (2000) 1716.
32. D.A. Fiedler and H.P. Fritz, *Electrochimica Acta* **40** (1995) 1595.
33. V. Dzhagan *et al*., *Nanoscale Research Lertets* **6** (2011) 79.
34. O.R. Ochoa, E.J. Witcowski III, C. Colajakomo, J.H. Simmons, and B.J. Potter Jr, *Journal of Materials Science Letters* **16** (1997) 613.
35. A. Dieguez, A. Romano-Rodríguez, A. Vilá, and J.R. Morante, *Journal of Applied Physics* **90** (2001) 1550.
36. I. Zardo *et al*., *Physical Review B* **80** (2009) 245324.
37. C. Trallero-Giner, A. Debernardi, M. Cardana, E. Menéndez-Proupin and A.I. Ekimov, *Physical Review B* **57** (1998) 4664.